Journal of Material Cycles and Waste Management (2026) 28:2471–2486
https://doi.org/10.1007/s10163-026-02573-9

ORIGINAL ARTICLE

# Impact of curing parameters on the properties of geopolymers derived from different class F fly ashes

Cemal Karaaslan[1] · Canan Turan[2] · Celal Tiltay[3]

Received: 4 December 2025 / Accepted: 13 April 2026 / Published online: 19 April 2026


## Abstract

This study investigates the effect of curing temperature and duration on the properties of Class F fly ash-based geopolymers (FGPs). FGP samples produced from three different fly ash sources were cured under various temperatures (ambient, 60 °C, 75 °C, and 90 °C) and durations (8, 24, 72, and 168 h). The compressive strength development, phase characterisation (FTIR and XRD) and microstructural evaluations (SEM and MIP) were performed. The major results reveal that although the chemical compositions of the fly ashes are quite similar, properties such as particle size distribution and particle morphology have a substantial impact on the properties of the FGPs. Fly ashes with a particle size distribution in a narrow range and mostly spherical morphology show higher reactivity, thereby minimising the requirement for extreme curing conditions. Therefore, FGPs produced with high-reactivity fly ash achieved high strength even at lower curing temperatures and shorter durations.

**Keywords** Fly ash · Particle size distribution · Geopolymer · Compressive strength · Phase characterisation

## Introduction

The need for concrete as a construction material is gradually increasing [1]. The production of Ordinary Portland Cement (OPC), which is a constituent of concrete, is also increasing in parallel with the demand for concrete. Global production of OPC has approached 4 billion tonnes annually [2]. However, serious environmental concerns emerge during this production, especially due to the greenhouse gas emissions [3]. For example, for every tonne of OPC produced, approximately 0.7–1.1 tonnes of carbon dioxide ($CO_2$) is released into the atmosphere, causing global warming [4–8]. Further, the OPC production causes nitric oxide emission, leading to acid rains [4]. Therefore, the development of new binders as alternatives to OPC is critical to maximise environmental benefits [9]. In recent years, geopolymers have been developed as promising alternatives to OPC, primarily because of their eco-friendly characteristics [10]. They also present enhanced mechanical properties and stability in volume [4], show high resistance to acid attacks and elevated temperatures [1], and represent high early strength [11].

Geopolymers are generally characterised as amorphous aluminosilicate cementitious materials [12]. They are formed through the reaction of aluminosilicate materials with alkali activators [9]. Geopolymerisation is a polymeric reaction that relies on the alumino-silica chain, occurring when a specific quantity of alumina and silica reacts in an alkaline solution. This process is commonly termed as alkali activation, a process that transforms the amorphous components of materials into a composite with strong binding properties [11]. Even though studies are being conducted to fully understand all the processes of alkali activation with aluminosilicates, the most widely accepted process for geopolymerisation can be summarised in three steps [4, 13]: (i) the dissolution of amorphous aluminosilicate materials at high pH, (ii) transportation of precursor ions into monomers, and (iii) condensation of monomers into polymers and hardening into geopolymer structure.

✉ Cemal Karaaslan
cemal.karaaslan@igdir.edu.tr; cemalkaraas@gmail.com

[1] Igdir Vocational School of Technical Sciences, Igdir University, Igdir 76000, Turkey

[2] Department of Civil Engineering, Faculty of Engineering and Architecture, Kirsehir Ahi Evran University, Kirsehir 40100, Turkey

[3] Department of Mechanical Engineering, Faculty of Engineering, Igdir University, Igdir 76000, Turkey

To produce geopolymers, a wide range of naturally occurring and industrially produced aluminosilicate materials can be used as precursors [9, 14]. Among these, the most commonly used precursors are calcined clays, ground granulated blast furnace slag, and fly ash. However, calcined clays are less preferable because of their plate-shaped particles, leading to high water demand and porosity in concrete production [15]. In addition, as a hazardous waste, the need to recycle slag is significantly lower compared to fly ash [16]. Therefore, fly ash, known as industrial by-product, is a more suitable precursor for the geopolymerisation [1].

Fly ash is a by-product produced in thermal power plants through the combustion of coal [17, 18]. In many countries, fly ash is generated in large amounts, with over 65% of this by-product currently being disposed of in landfills [19]. John et al. [9] indicated a global annual production of approximately 780 million tonnes of fly ash, with only about 17–20% being effectively utilised. This inadequate management of fly ash as a waste material poses potential risks of severe environmental and health issues [20]. Moreover, fly ash production continues to increase in countries such as China, India, and Turkey where coal-fired power plants are dominantly used for electricity generation [16].

Curing conditions represent one of the critical parameters influencing the geopolymerisation process [2]. In an alkaline environment, the dissolution rates of binders such as slag and metakaolin are high [21, 22], class F fly ash dissolves at a moderate rate [11, 23], and natural pozzolans dissolve at a slower rate [24, 25]. To this direction, the need for curing temperature and duration increases in relation to the rate of dissolution. The geopolymerisation process of a fly ash-based geopolymer (FGP) is quite slow at ambient temperature, whereas the rate of the reaction process accelerates with an elevated temperature [11, 26].

Table 1 provides an overview of previous studies on how curing temperature, curing duration and testing age affect FGPs, and also lists the curing conditions that those studies considered to be optimal. In several studies, strength increases were observed at temperatures or durations higher than the recommended values, and some included partial replacement of fly ash, which may have affected the reported outcomes. For this reason, it is difficult to define a single curing regime that is applicable in all cases. Nevertheless, most studies indicate that low-calcium fly ashes generally perform best within a curing range of about 60–90 °C. Variations within this range are mainly associated with differences in activator composition and fly ash chemistry. However, even fly ashes with similar chemical compositions may require different curing conditions due to differences in particle size, morphology, surface area, amorphous content and dissolution behaviour.

Most earlier literature has concentrated on the chemical composition of individual low-calcium fly ashes, while the roles of their physical and microstructural characteristics have received far less attention. This study addresses this gap by examining three low-calcium fly ashes from the Catalagzi, Iskenderun and Sugozu power plants, which show similar chemical compositions but differ in several key properties. These materials were characterised using specific surface area measurements, Blaine and BET analyses, scanning electron microscopy (SEM), X-ray diffraction (XRD) and nitrogen adsorption. The first aim of the study is to investigate how these characteristics influence the compressive strength of FGPs, rather than relying solely on chemical composition. Compressive strength was assessed at 28 days for all sources, and extended to 3, 7 and 90 days for Catalagzi fly ash, which is unique in Türkiye for its use of domestically mined bituminous coal.

Although many studies have proposed curing ranges for improving FGP strength, the most suitable combination of curing temperature and duration remains uncertain. Therefore, the second aim of this work is to examine how these two parameters affect the mechanical and microstructural development of Catalagzi FGPs synthesised with sodium silicate and sodium hydroxide solutions. Samples were cured at ambient temperature, 60 °C, 75 °C and 90 °C for 8, 24, 72 and 168 h. Compressive strength testing was supported by Fourier transform infrared spectroscopy (FTIR), XRD, SEM and mercury intrusion porosimetry (MIP) analyses to provide insight into microstructural evolution and pore characteristics.

## Experimental programme

### Materials

Three different Class F fly ashes were used to produce FGPs. The first one was obtained from Catalagzi Thermal Power Plant (Zonguldak, Türkiye), the only power plant that uses domestic bituminous coal as fuel in the country. The second and third fly ashes were obtained from Iskenderun Thermal Power Plant (Hatay, Türkiye) and Sugozu Thermal Power Plant (Adana, Türkiye), respectively. The fly ashes used in this study were sourced from Turkish thermal power plants employing typical pulverised coal combustion technologies; fluidised bed combustion systems were not considered within the scope of this study. The locations where these three fly ashes were obtained are shown with the regional and global scales in Fig. 1.

The chemical compositions determined by wet-chemical analysis of fly ashes are presented in Table 2. It is evident that the contents of CaO, $SiO_2$, $Al_2O_3$, and $Fe_2O_3$, which are

**Table 1** Literature review on curing temperatures, durations, and testing age for class F fly ash-based geopolymers

| References | Curing temperature range (°C) | Curing time range (h) | Optimum curing condition | Testing age (days) |
|---|---|---|---|---|
| Palomo et al. 1999 [27] | 65 and 85 | 2, 5, and 24 | 85 °C for 5/24 h | Single age (after curing) |
| Swanepoel and Strydom 2002 [28] | 40, 50, 60, and 70 | 6, 24, 48, and 72 | 60 °C for 48 h | 7 and 28 |
| Criado et al. 2005 [29] | 85 | 5, 12, 20, and 168 | - | Single age (unspecified) |
| Hardjito and Rangan 2005 [30] | 30, 45, 60, 75, and 90 | 4, 6, 8, 12, 24, 48, 72, and 96 | - | 3, 7, 14, 28, 56, and 91 (only for specific curing conditions) |
| Sindhunata et al. 2006 [31] | 30, 50, and 75 | 24 and 48 | - | No strength results. |
| Vora and Dave 2013 [32] | 60, 75, and 90 | 24, and 48 | Studied separately. | 3 and 7 (only for specific curing conditions) |
| Adam and Horianto 2014 [33] | Ambient, 80, 100, and 120 | 4, 6, and 20 | 120 °C for 20 h | 3, 7, 14, and 28 |
| Atiş et al. 2015 [11] | 45, 55, 65, 75, 85, 95, 105, and 115 | 24, 48, and 72 | 115 °C for 24 h | 1 for 24 curing time; 2 for 48 curing time; 3 for 72 curing time |
| Nagalia et al. 2016 [34] | Oven-curing: 55 and 70 °C; Steam-curing: 46 °C; Ambient-curing: 25 °C | 24, 72, and 168 | 70 °C for 48 h | 1, 7, and 28 (Only for specific curing conditions) |
| Görhan et al. 2016 [21] | 60 and 80 | 2,4, and 24 | 60 °C for 2 h | 7 |
| Aliabdo et al. 2016 [35] | 28, 50, 70, and 90 | 24, 48, and 72 | 70 °C for 48 h | 7 and 28 |
| Zhang et al. 2018 [36] | At ambient temperature, at 50 °C for 168 h, and at 80 °C for 24 h | | - | 2, 7, 14, 28, 49, 90, and 120 |
| Hassan et al. 2019 [37] | Ambient, 75 | 26 | 75 °C for 26 h | 7, 28, 56, 90, and 180 |
| Kuenzel and Ranjbar 2019 [38] | 25, 45, 65, 85, 105, 125, 145 | 1, 2, 4, 6, 12, and 24 | - | No strength results. |
| Sajan et al. 2021 [39] | 20, 40, 60, and 80 | 72, 168, and 336 | 60 °C for 168 h | 14 |
| Rabie et al. 2022 [40] | Ambient, 40, 80, and 120 | 24, 48, and 72 | 80 °C for 24 h | 1, 3, 7, and 28 (only for ambient and 80 °C for 24 h) |
| Gopalakrishna and Dinakar 2023 [2] | Ambient, 60, 80, and 100 | 24 | 80 °C for 24 h | 3, 7, 28, 56, and 90 |
| Yılmaz et al. 2023 [23] | Ambient, 40, 60, and 80 | 24, 48, and 72 | 80 °C for 72 h | 2, 7, and 28 |
| Karaaslan et al. 2025 [25] | Ambient (25 °C), high-ambient (45 °C), and heat-curing (at 75 °C for 24 h) | | High-ambient curing | 3, 7, 28, and 90 |

[29] Strength continued to increase with curing time, reaching higher values up to 168 h

[30] The full range of curing temperature and duration combinations was not investigated. Increasing temperature enhances strength, but improvement is limited above 60 °C. At 60 °C, longer curing time increases strength noticeably up to 24 h

[21] Metakaolin was used as a replacement for fly ash at 10%, 20%, 30%, and 40%

[35] OPC was used as a replacement for fly ash at 5%, 10%, and 15%. Also, curing at 70 °C for 72 h was not tested

[36] Red mud was used as a replacement for 25% fly ash

[39] Curing at 60 °C for 168 h was optimal, as 80 °C and 336 h offered no significant strength gain

critical for geopolymerisation in powder binders, are largely comparable across the three fly ashes.

In order to activate the fly ashes, a mixture consisting of commercial-grade sodium hydroxide (with 98% purity) and sodium silicate (with a weight ratio of $SiO_2/Na_2O = 2.04$ and a $SiO_2$ content of 24.50%) was used. The sodium hydroxide was dissolved in distilled water to obtain a 10 M NaOH solution, which was then left to rest for 24 h before use. Subsequently, it was added to the sodium silicate solution, and after 5 min of stirring, the mixture was allowed to stand for half an hour. After this period, finally, the mixture was added to the solid material consisting of fly ash and sand.

In addition, sand (with a maximum particle size of 4.75 mm) obtained from the local river deposits was utilised as aggregate. This sand has a specific gravity of 2.71 and a water absorption rate of 1.6%. The sand used in this study was graded in accordance with ASTM C144-04 [41].

## Sample preparation and curing

In terms of samples, three different FGP mortar mixtures were prepared with three different fly ashes. Based on the same consistency, the mixing ratios were selected as shown in Table 3. Also, the weight ratio of sodium silicate solution to 10 M NaOH solution used in these mortars was 2.5 for all mixtures. The weight ratio of the alkali activator solution to fly ash was 0.50 for Catalagzi and Iskenderun, and 0.35 for Sugozu.

The mixing process for all mixes was conducted in the same way. The fly ash and sand were firstly mixed in

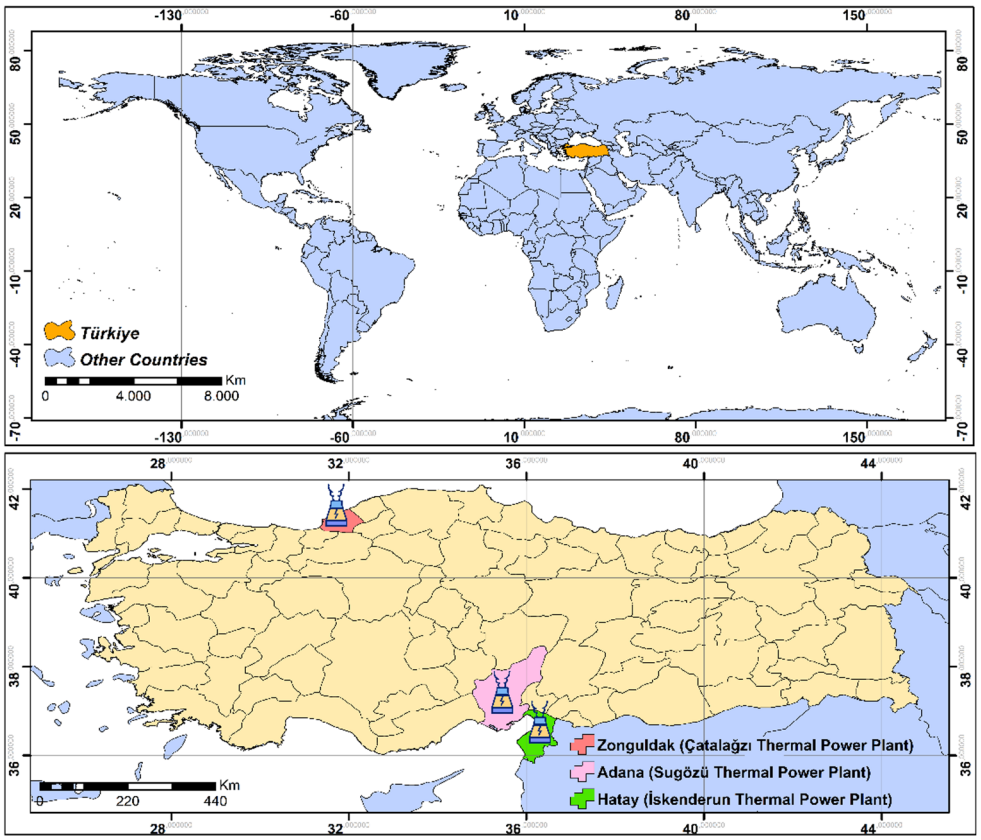


**Fig. 1** Locations of thermal power plants where the fly ashes were collected, global and Türkiye regional scales

**Table 2** Chemical compositions of fly ashes (wt%)

LOI: Loss on ignition

| Fly ashes | CaO | $SiO_2$ | $Al_2O_3$ | $Fe_2O_3$ | MgO | $Na_2O$ | $K_2O$ | $SO_3$ | LOI |
|---|---|---|---|---|---|---|---|---|---|
| Catalagzi | 2.46 | 55.51 | 23.09 | 6.64 | 1.58 | 0.14 | 3.56 | 0.24 | 1.63 |
| Iskenderun | 3.17 | 58.36 | 25.57 | 6.85 | 1.97 | 0.09 | 1.49 | 0.04 | 1.26 |
| Sugozu | 3.75 | 55.98 | 21.19 | 6.94 | 2.45 | 1.91 | 2.42 | 0.42 | 2.14 |

**Table 3** Mix proportions of FGP mortars (g)

| Mix ID | Sodium hydroxide solution | Sodium silicate solution | Fly ash | River sand |
|---|---|---|---|---|
| Catalagzi-FGP | 64.3 | 160.7 | 450 | 1350 |
| Iskenderun-FGP | 64.3 | 160.7 | 450 | 1350 |
| Sugozu-FGP | 45.0 | 112.5 | 450 | 1350 |

a cement mixer for 2 min. Then, the previously prepared alkali activator mixture was added to the mixture of solids, and the mixing was continued for another 3 min. After this time, the fresh mortar was poured into the 40 mm plastic cube molds in 2 layers. For each layer, the cube molds were dropped 60 times on a jolting table. Once the placement and compaction processes were completed, the samples were wrapped in a special plastic bag to protect the moisture contents of the samples. Subsequently, the samples were placed in the oven at specified temperatures as soon as their surface finishing were completed.

At the end of the curing periods, the samples were removed from the molds and left in the laboratory (at 25 °C) until the day tests are conducted. It should be noted here that Catalagzi and Iskenderun FGP samples left at room temperature did not solidify sufficiently within the first 3 days, so their 3-day strengths could not be measured, and they were demolded after 6 days.

## Experimental methods

The compressive strengths of the Catalagzi FGPs at 3, 7, 28, and 90 days, as well as the Iskenderun and Sugozu FGPs at 28 days, were determined in accordance with TS EN 196-1 [42]. The compressive strength was determined based on the average of three specimens.

The particle size distribution of the raw fly ashes was analysed using a laser diffraction particle size analyser (Malvern Mastersizer 3000).

The nitrogen adsorption technique, using a Micromeritics Tristar II 3020 analyser, was applied to the raw fly ashes to determine their Brunauer–Emmett–Teller (BET) surface areas.

To determine the reactive Si and Al content of fly ash for geopolymerisation, 7.5 g of fly ash was mixed with 200 mL of 10 M NaOH solution in a closed beaker. The beaker was heated on a hot plate set to 75 °C, and the mixture was continuously stirred for 4 h using a magnetic stirrer. Afterward, the solution was filtered, and the filtrate was analysed using Inductively Coupled Plasma Optical Emission Spectroscopy (ICP-OES) to measure the Si and Al content [43, 44].

The Catalagzi FGP specimens used for determining the 28-day compressive strength were further analysed using FTIR, XRD, SEM, and MIP techniques. A portion of these samples, in their bulk form, was used for SEM and MIP analyses. The remaining portion was processed into a powdered state through grinding in a ring mill. The powdered materials were subsequently employed in FTIR and XRD analyses.

To observe the molecular bond structure of Catalagzi FGPs concerning curing temperature and time, the Agilent Cary 630 model FTIR spectrometer was employed. This instrument operated in the wavelength range of 4000–650 $cm^{-1}$.

The mineralogical composition of the Catalagzi FGPs was determined using the Tongda TD-3500 model XRD device. The samples were measured with 2θ range of 10° to 80° in the step size of 0.02°.

The microstructure of the raw fly ashes and Catalagzi FGPs was determined using a ZEIS Gemini Sigma 300 SEM.

The pore structure of the Catalagzi FGPs was analysed through mercury intrusion porosimetry (MIP) using a Quantachrome Pore Master 60 device. This method determined the pore size distribution within the range of 4 nm to 10 µm, utilising a high-pressure chamber capable of reaching up to 55,000 psi.

## Results and discussions

### Effects of characterisation for Catalagzi, Iskenderun, and Sugozu fly ashes

Fly ash sources usually contain some unburned carbon particles. These particles are typically larger than 100 µm, increasing the surface area due to their porous structure [45]. Beyond the presence of unburned carbon, fly ash does not consist of a uniform particle mixture. Excluding certain impurities, fly ash particles are generally classified into three main groups [38, 46]: (i) aluminosilicates with a high amorphous fraction, (ii) cenospheres, and (iii) metal oxides, such as quartz and iron oxides. Aluminosilicates are reactive particles that fully participate in geopolymerisation. These particles typically range in size from 1 µm to 100 µm, with the majority being smaller than 50 µm [47]. Cenospheres, on the other hand, are partially reactive particles with aluminosilicate shells that react in highly alkaline environments while their skeletal structure remains unreacted. These particles range from 10 µm to 500 µm, with most being smaller than 200 µm [48]. These hollow particles typically have a specific gravity of less than 0.8 [49, 50]. Metal oxide particles, however, are inert components that do not participate in geopolymerisation and remain unchanged within the matrix, typically ranging in size from 1 µm to 40 µm. In addition to these common particle types, submicron-sized particles associated with trace elements are also presented in fly ash sources [47].

Figure 2 presents the particle size distributions for the fly ashes used in this study. Table 4 presents the $D_{10}$, $D_{50}$, and $D_{90}$ values obtained from laser particle size distribution (LPSD) analysis, along with the specific surface area. Additionally, the Blaine surface area, BET surface area, and specific gravity values are provided. $D_{10}$ and $D_{90}$ values are 1.75 µm and 97.90 µm for Catalagzi, 2.83 µm and 107.00 µm for Iskenderun, and 3.87 µm and 82.10 µm for Sugozu, respectively. Catalagzi fly ash contains 7.42% particles

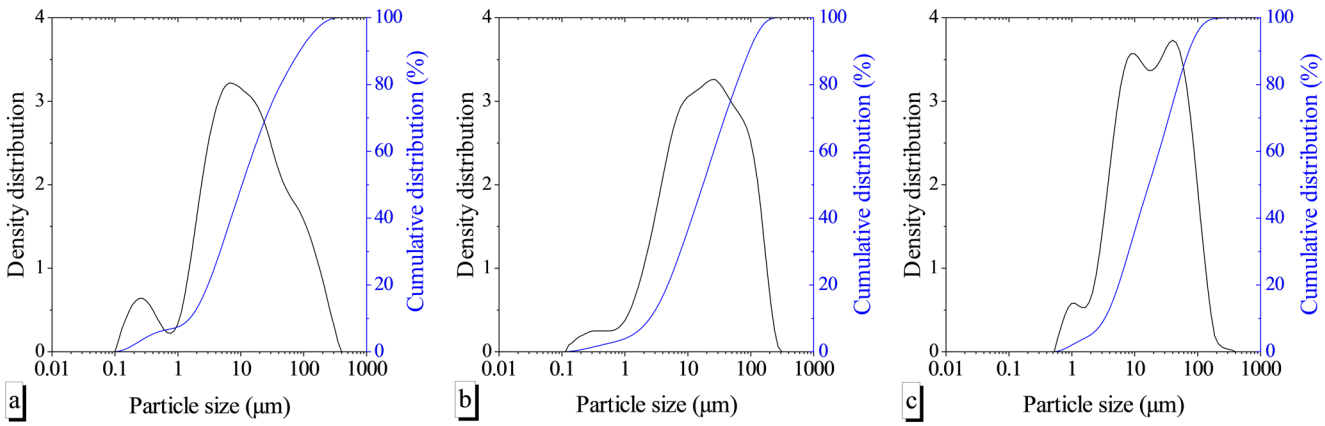


**Fig. 2** Particle size distributions of Catalagzi (**a**), Iskenderun (**b**), and Sugozu (**c**) fly ashes

**Table 4** Summary of fly ash characteristics: results of LPSD analysis, Blaine surface area, BET surface area, and specific gravity

| Fly ashes | $D_{10}$ (μm) | $D_{50}$ (μm) | $D_{90}$ (μm) | Surface area of LPSD ($cm^2/g$) | Blaine specific surface area ($cm^2/g$) | BET surface area ($cm^2/g$) | Specific gravity |
|---|---|---|---|---|---|---|---|
| Catalagzi | 1.75 | 11.80 | 97.90 | 16,380 | 3805 | 19,800 | 2.13 |
| Iskenderun | 2.83 | 19.70 | 107.00 | 12,080 | 3295 | 11,300 | 2.12 |
| Sugozu | 3.87 | 19.00 | 82.10 | 7220 | 3004 | 10,850 | 2.34 |

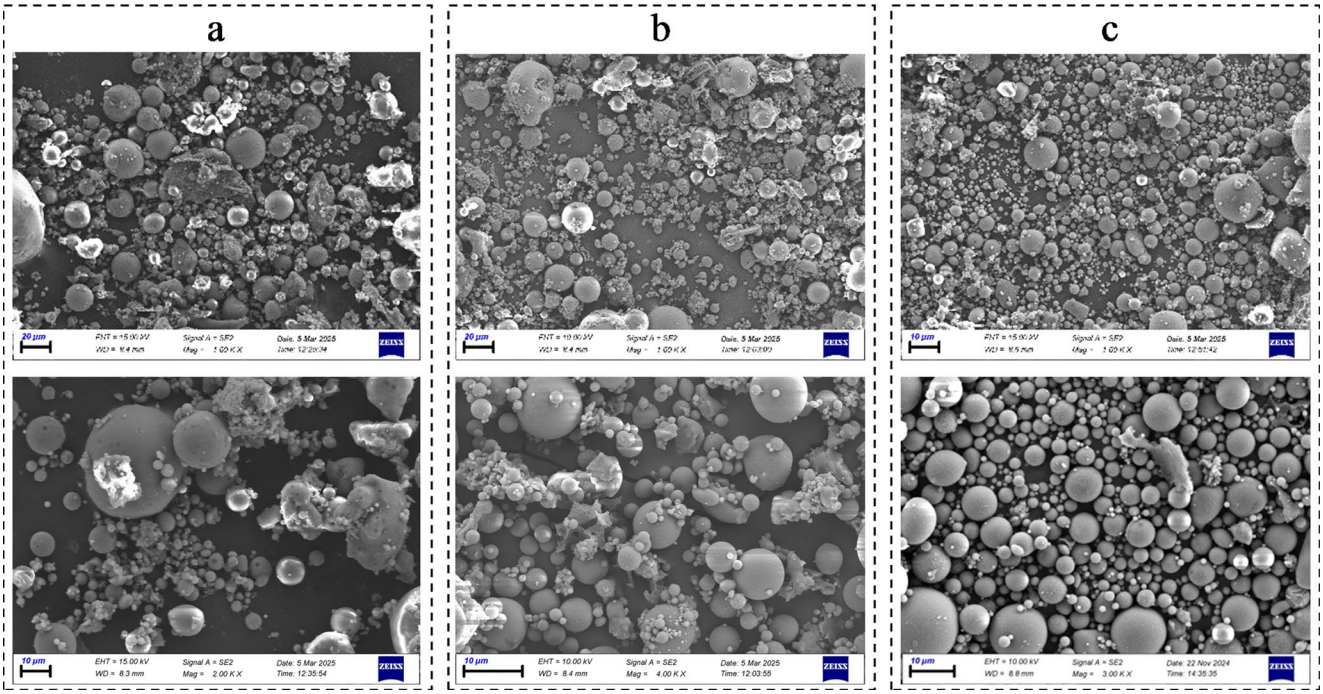


**Fig. 3** SEM micrographs of Catalagzi (**a**), Iskenderun (**b**), and Sugozu (**c**) fly ashes

smaller than 1 μm and 8.38% particles larger than 100 μm. Iskenderun fly ash contains 3.91% particles smaller than 1 μm and 9.20% particles larger than 100 μm. On the other hand, Sugozu fly ash contains 2.00% particles smaller than 1 μm and 4.40% particles larger than 100 μm. Sugozu fly ash has a higher proportion of particles in the 1–100 μm range, indicating the presence of more reactive aluminosilicate particles. Moreover, the specific gravity of Sugozu fly ash is higher than that of the other two. The lower specific gravity of Catalagzi and Iskenderun fly ashes suggests that these materials may contain more low-density cenospheres compared to Sugozu fly ash [49–51].

When comparing the specific surface area, Blaine surface area, and BET surface area, Sugozu fly ash exhibits a lower surface area. This observation indicates the presence of irregular particle shapes and some unburned organic matter in Iskenderun and particularly Catalagzi fly ashes [52]. The lower surface area of Sugozu fly ash also explains why Sugozu FGP mixtures achieve similar consistency with lower alkali activator content compared to two other FGP mixtures (Table 3).

SEM images of fly ashes are shown in Fig. 3. In general, spherical particles are predominant in all samples, but Sugozu fly ash is observed to have more uniformly spherical particles. This also explains the low surface area of Sugozu fly ash (Table 4).

The XRD patterns of the fly ashes are shown in Fig. 4. In general, the fly ashes consist predominantly of an amorphous phase together with crystalline mullite, quartz, and hematite. Compared with the Catalagzi and Iskenderun fly ashes, the Sugozu fly ash shows lower apparent intensities for several crystalline peaks, particularly those associated with mullite and hematite, suggesting lower apparent crystallinity under the present test conditions. Based on this qualitative observation, and when considered together with the SEM observations, particle size distribution, surface area measurements, dissolved Si and Al contents, and strength results, this may be associated with a higher amorphous phase content in the Sugozu fly ash.

Figure 5 illustrates the dissolved Si and Al quantities after immersing the fly ashes in a 10 mol NaOH solution at 75 °C for 4 h. As can be seen, the amounts of dissolved Si

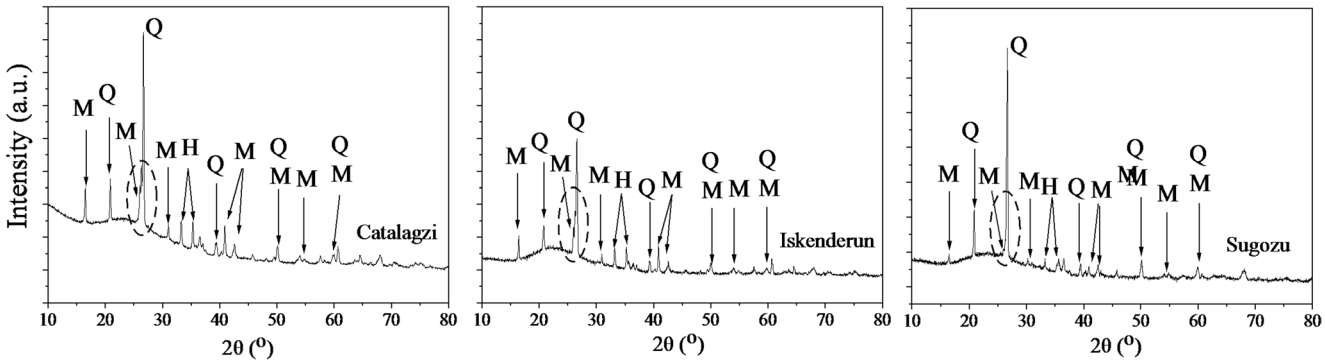


**Fig. 4** XRD patterns of fly ashes; M=mullite, Q=quartz, H= hematite

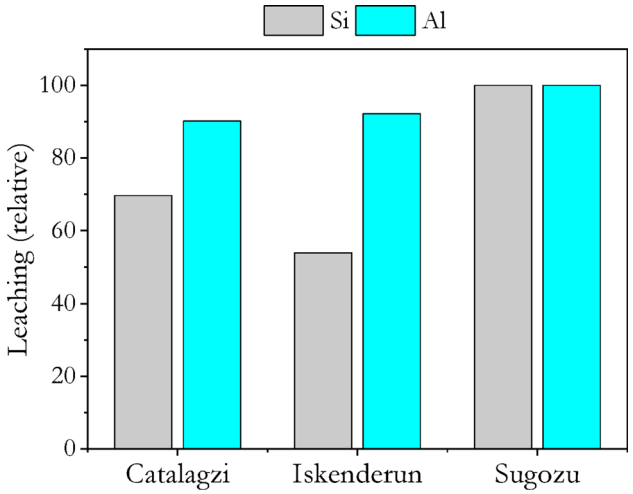


**Fig. 5** Dissolved Si and Al amounts of three different fly ashes in NaOH solution

and Al for Sugozu fly ash are higher than those of the other two fly ashes. This indicates that Sugozu fly ash contains higher quantities of reactive Si and Al.

Based on the combined evaluation of LPSD and nitrogen adsorption analyses, SEM images, XRD patterns, and Si/Al solubility in NaOH solution, Sugozu fly ash is concluded to be more reactive than the other two fly ashes. Fly ashes with different reactivities are also expected to respond differently to varying curing temperatures and durations.

## Compressive strength

### Strength development of Catalagzi FGPs over 90 days

The 3, 7, 28, and 90-day compressive strengths of Catalagzi FGPs cured at ambient temperature were 0.0, 2.8, 21.2, and 28.2 MPa, respectively. These results indicate that the strength development of Catalagzi FGPs cured at ambient temperature progresses slowly [40, 53]. Slow strength gain is due to the slow alkali activation of fly ash at low temperatures. Studies have shown that the alkali activation of fly ash in NaOH solution at 20 °C can be approximately 70 times slower than at 60 °C [54, 55]. Consequently, slow geopolymerisation at low temperatures causes very slow strength gain and low ultimate strength, as seen in Catalagzi FGPs. The low ultimate strength at ambient-curing highlights the importance of elevated temperatures for activating low-calcium fly ashes [38, 56, 57].

The 90-day compressive strength development of Catalagzi FGPs cured at different temperatures and durations is presented in Fig. 6. Note that the 3-day strength of 7-day cured specimens is assumed equal to that of 3-day cured specimens. As seen from Fig. 6, the compressive strength of the specimens that are cured for 8 h increases significantly over time. Specifically, the strength of the specimens cured for 8 h at the temperatures of 60 °C, 75 °C, and 90 °C rise 214.5%, 125.1%, and 119.8% from 3 days to 90 days, respectively. In contrast, specimens cured for 3 and 7 days show little increase, especially after 28 days.

The fresh FGP paste consists of fly ash particles with alkali activator-filled voids. The reaction products formed by the geopolymerisation fills these voids. As a result, the voids are partially filled with geopolymer gels. The degree of filled voids has a major impact on the strength and durability of FGPs. The progress in the formation of geopolymerisation products, which decrease the number of voids, is directly affected by temperature. At higher temperatures, reactions are faster, causing rapid solidification and high early strength. However, rapid solidification forms larger pores, resulting in a less ordered structure [53, 58, 59]. Although curing at 90 °C enhances early strength, the degree of geopolymerisation stabilises at levels similar to those achieved at lower curing temperatures over time. Consequently, the less ordered structure dominates at later stages, limiting the final compressive strength [58, 60, 61].

As shown in Fig. 6, Catalagzi FGPs cured at 90 °C for 3 days or longer achieved significant strength within the first 3 days, with only limited additional gain afterward. Consequently, their ultimate strengths were lower than those cured at 60–75 °C for the same period. Furthermore, the higher the

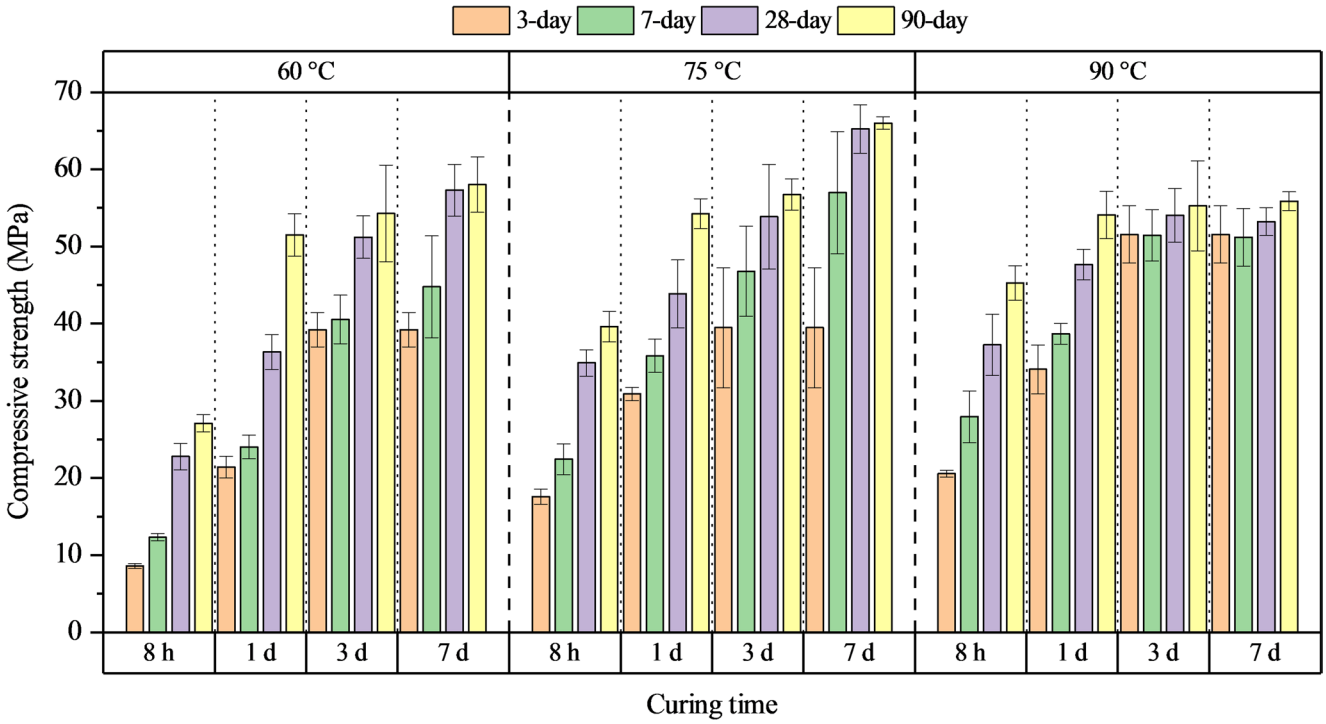


**Fig. 6** Compressive strength development of Catalagzi FGPs under various curing temperatures and durations

reactivity of an aluminosilicate source, the more sensitive it becomes to the negative effects of elevated curing temperatures. It may also be adversely affected by relatively lower curing temperatures (as discussed in Sect. 3.2.2). Therefore, it should be noted that the curing temperature at which different fly ashes are negatively affected varies depending on their reactivity. For Catalagzi fly ash (and others with similar reactivity), a moderate curing temperature of 60 °C to 75 °C is required to achieve sufficient activation and to form a more uniform, less porous matrix with well-distributed reaction products. These FGPs also exhibit higher frost resistance due to reduced permeability [23].

In terms of curing duration, it is well-known that extending the thermal curing time increases the formation of reaction products and enhances the degree of cross-linking in the three-dimensional aluminosilicate network [62]. This leads to improvements in the strength. However, 28-day compressive strength results show that at 90 °C, extending curing beyond 24 h yields only marginal gains and may cause strength loss after 72 h. Similar observations have been reported in other studies [24, 40, 63]. This suggests that Catalagzi FGPs (and similar fly ashes) nearly complete their geopolymerisation within 28 days when cured at 90 °C for 24 h or longer. The strength loss observed beyond 72 h can be attributed to the accelerated release of water from the geopolymeric network at elevated curing temperatures due to the higher reaction rate [36], which may generate internal voids and promote shrinkage cracking caused by drying shrinkage [24, 64, 65]. It should also be noted that with highly reactive fly ashes, the threshold curing duration at high temperatures—beyond which strength loss occurs—decreases (Sect. 3.2.2).

For Catalagzi FGP, samples cured at 90 °C for ≥ 3 days achieve very high strength quickly, indicating that 3 days at 90 °C is optimal for early strength. On the other hand, considering the early age of 7 days for concrete, curing at 75 °C for 7 days can be considered optimal, providing a strength of 57.0 MPa. However, for structures where impermeability is as critical as strength, curing at 60 °C for 7 days may be more suitable [36, 58]. These findings suggest that the optimal curing conditions for FGPs depends on specific application requirements, such as achieving early high strength, long-term durability, low porosity, or energy and cost savings [36].

### 28-day strengths of Catalagzi, Iskenderun, and Sugozu FGPs

The 28-day compressive strengths of Catalagzi, Iskenderun, and Sugozu FGPs cured at ambient temperature were measured as 21.2 MPa, 22.7 MPa, and 34.3 MPa, respectively. Additionally, Fig. 7 presents the 28-day compressive strengths of FGPs under varying curing temperatures and durations. At the mildest curing condition (60 °C for 8 h), the compressive strengths of Catalagzi and Iskenderun FGPs, at 22.8 MPa and 23.2 MPa respectively, exhibit

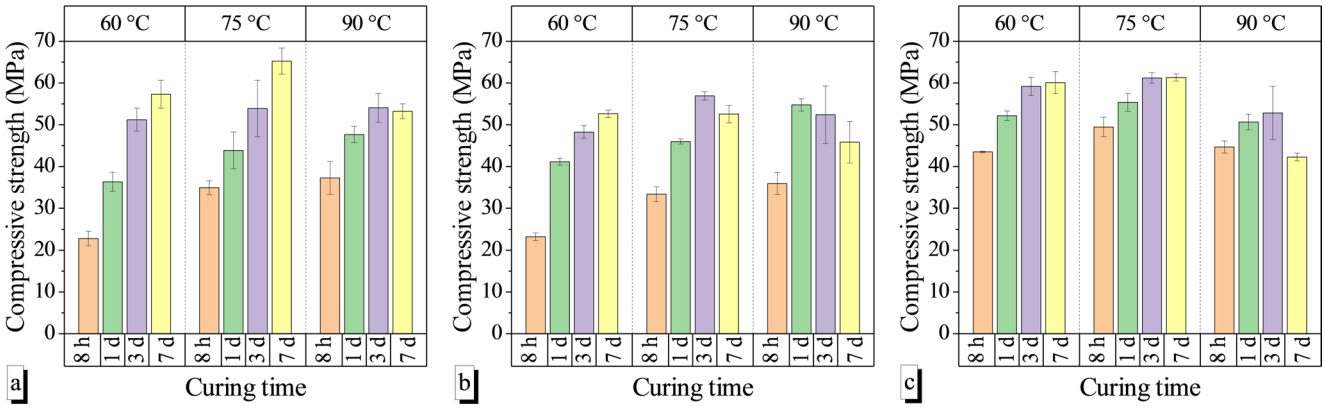


**Fig. 7** Compressive strength at 28 days of Catalagzi (**a**), Iskenderun (**b**), and Sugozu (**c**) FGPs cured at different temperatures and durations

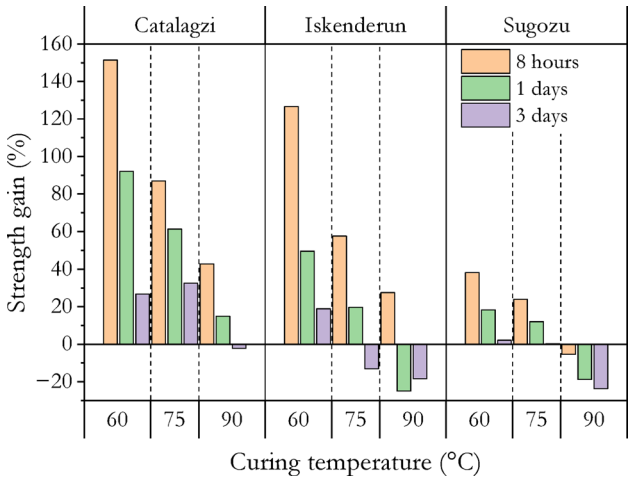


**Fig. 8** Percentile compressive strength gain comparison of FGPs cured for 8 h, 1 day, and 3 days (compared to those cured for 7 days)

little difference from those cured at ambient temperature. In contrast, the Sugozu FGP shows a 26.8% increase, reaching 43.5 MPa. Sugozu FGP achieves higher strength at ambient temperature compared to the other two and exhibits significant strength improvement even under low thermal curing conditions. This suggests that the Sugozu fly ash, which is more reactive than the other two, requires relatively less thermal curing. Furthermore, the ability of Sugozu FGP to achieve high strength under other mild curing conditions (60 °C for 1 day, 75 °C for 8 h, 75 °C for 24 h, and 90 °C for 8 h) supports this conclusion.

Compressive strength of all three FGPs generally increases with longer curing at 60 °C and 75 °C, though the rate differs among fly ashes. To illustrate this, Fig. 8 compares the strengths of samples cured for 8 h, 1 day, and 3 days relative to those cured for 7 days. As observed, Catalagzi and Iskenderun FGPs cured for 7 days show much higher strength than those cured for 8 h. Specifically, for Catalagzi FGPs at 60 °C, 75 °C, and 90 °C, the increases are 151.4%, 86.9%, and 42.9%, and for Iskenderun FGPs, 126.7%, 57.5%, and 27.5%, respectively. It is evident that the influence of prolonged curing on strength improvement diminishes with higher temperatures. This outcome is supported by a study conducted by Sajan et al. [39], which stated that the geopolymerisation reactions of fly ashes are primarily influenced by curing temperature, and curing durations exceeding 3 days at temperatures above 60 °C do not result in a significant increase in strength. However, at 75 °C, this applies to Iskenderun FGPs but not Catalagzi FGPs (Fig. 8). Additionally, Atis et al. [11] noted that curing at 75 °C for over 2 days may reduce FGP strength. Similarly, Sugozu FGPs show limited strength gain with prolonged curing, even at low temperatures. Furthermore, extending curing from 8 h to 7 days at 90 °C increases strength in Catalagzi and Iskenderun FGPs, but reduces it in Sugozu FGPs.

This variability, also observed in other studies (e.g. [32]), , is primarily attributed to the reactivity of the fly ash, aside from factors such as the concentration of the alkaline activator. Sugozu FGP, with higher reactivity, achieves high strength even at low temperatures and short curing times. In contrast, Iskenderun and especially Catalagzi FGPs require higher temperatures and/or longer curing. For instance, to reach 42.5 MPa, Catalagzi and Iskenderun FGPs need 60 °C for ≥ 3 days or 75–90 °C for ≥ 1 day, whereas Sugozu FGP reaches the same strength with only 8 h at 60 °C.

Although the chemical compositions of the three fly ashes are quite similar, the strengths of these FGPs indicate that their curing requirements for geopolymerisation vary. As discussed in Sect. 3.1, Sugozu fly ash contains a higher proportion of particles within the 1–100 µm size range, with a $D_{90}$ value of 82.1 µm, indicating that about 90% of its particles are smaller than 100 µm. At the same time, Fig. 2 shows that the fraction of particles finer than 1 µm in Sugozu fly ash is relatively low (2.00%), suggesting that its particle size distribution is mainly concentrated within the 1–100 µm range. The abundance of particles in this size range may enhance the reactivity of aluminosilicate phases and therefore reduce the need for elevated curing temperatures [47].

Similarly, Gao et al. [66] reported that particle size distribution affects reaction activity more than amorphous content or average particle size.

One of the key advantages of fly ash particles being mostly smooth and spherical within a narrow size range is their relatively low total surface area. This characteristic reduces the amount of alkaline activator required to achieve adequate workability in geopolymers (Table 3). Since the alkaline activator is typically the most expensive component and one of the main contributors to the environmental impact of geopolymer systems, reducing the activator demand can significantly improve their economic and environmental performance [67–69]. Previous life-cycle and cost analyses have shown that alkaline activator production is the dominant driver of both the environmental impacts and production costs of geopolymer concrete [70–72]. Furthermore fly ashes rich in such particles also need lower curing temperatures and shorter durations, further reducing energy use and emissions [73]. Therefore, Sugozu FGPs are expected to be more cost-effective and environmentally friendly than those from other fly ashes.

## Analysis of reaction products

### Fourier-transform infrared (FTIR)

The chemical bonding of Catalagzi FGP cured at different temperatures and durations are characterised by FTIR. As can be seen in Fig. 9, the main FTIR bands of all FGPs are between 1300 and 800 $cm^{-1}$, indicating asymmetric Si-O-T (T = Si or Al) stretching [38, 74]. The main band at 1018 $cm^{-1}$ in raw fly ash narrows and shifts to lower wavenumbers during alkali activation, showing dissolution of Si and Al monomers in early geopolymerisation. This process takes several days at ambient temperature or several hours at elevated temperatures. Since the FTIR spectrum in the study is

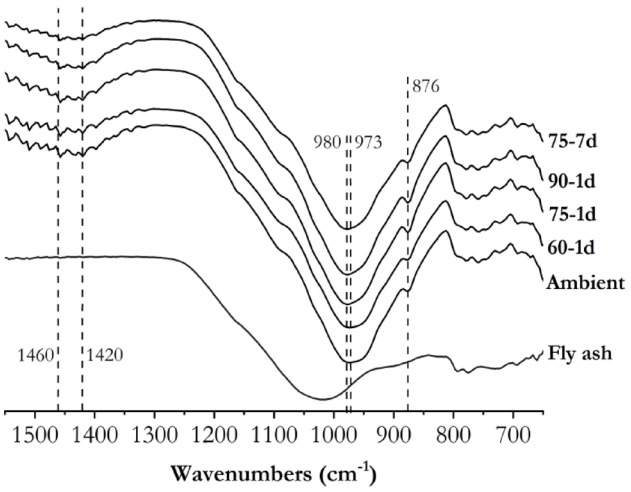


**Fig. 9** FTIR spectra of raw Catalagzi fly ash and Catalagzi FGPs

obtained at 90 days, and considering that the later phases of geopolymerisation are nearly complete by this time, the following conclusion can be drawn [36]: The initial broad band of raw fly ash shifts lower due to the dissolution of Si and Al monomers from the raw material during the process from mixing to solidification. In the second phase, slight shifts to higher wavenumbers occur as silicate and aluminate oligomers polymerise. In the final phase of geopolymerisation, the formation of Si-rich cross-linked tectosilicate gel is anticipated to shift the main bands to lower wavelengths and eventually reach wavelengths below those of raw fly ash. Evaluating FGP spectra shows that increasing curing temperature and duration generally shifts the main band to higher wavenumbers: 973, 974, 977, 978, and 980 $cm^{-1}$ for the AMB, 60-1d, 75-1d, 90-1d, and 75-7d, respectively, indicating more cross-linked geopolymer gels [29, 36, 39].

Weak bands between 1460 and 1420 $cm^{-1}$ observed in the FGPs—but not in raw fly ash—indicate asymmetric O–C–O stretching vibrations [24, 75]. These bands show that excess $Na^+$, which does not participate in geopolymerisation, reacts with atmospheric $CO_2$ to form $Na_2CO_3$. This band is more prominent in samples cured at ambient temperature and at 90 °C. At ambient temperature, lower reaction progress leaves more unreacted $Na^+$ and insufficient filling of voids, and the higher permeability allows $CO_2$ to penetrate and increase carbonation. At 90 °C, high carbonation is linked to increased permeability caused by voids formed due to water evaporation (see Sect. 3.2). In contrast, the reduced band intensity in samples cured at 75 °C for 7 days likely reflects sufficient reaction product formation and lower permeability.

A band at 876 $cm^{-1}$, which is absent in the fly ash spectrum but present in FGPs, may indicate (i) Si–O terminal bond vibrations [38, 76], or (ii) the formation of sodium bicarbonate [29, 75].

Another band that is not present in the fly ash spectrum but appears in the FGP spectrum is located at 876 $cm^{-1}$. This may indicate two conditions: (i) Si-O terminal bond vibrations [38, 76], or (ii) the formation of sodium bicarbonate [29, 75]. The first suggests increased crystallinity of cenosphere and metal oxide particles, which do not participate in geopolymerisation [38, 46]. The second reflects carbonation resulting from exposure to atmospheric $CO_2$ [77].

### X-ray diffraction (XRD)

Figure 10 shows the XRD patterns of raw Catalagzi fly ash and Catalagzi FGP cured at ambient temperature. The raw fly ash exhibits a predominantly amorphous phase together with crystalline quartz, mullite and hematite, whereas the ambient-cured FGP is characterised mainly by quartz- and mullite-related reflections. The main amorphous phase of

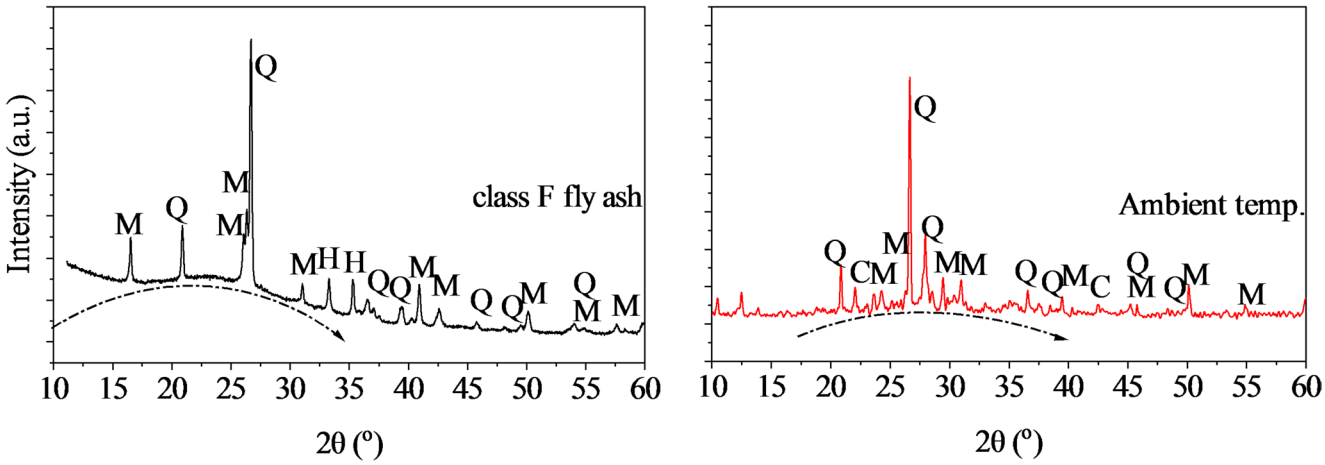


**Fig. 10** XRD patterns of Catalagzi fly ash and Catalagzi FGP at ambient temperature; M=mullite, Q=quartz, H=hematite, C=calcite

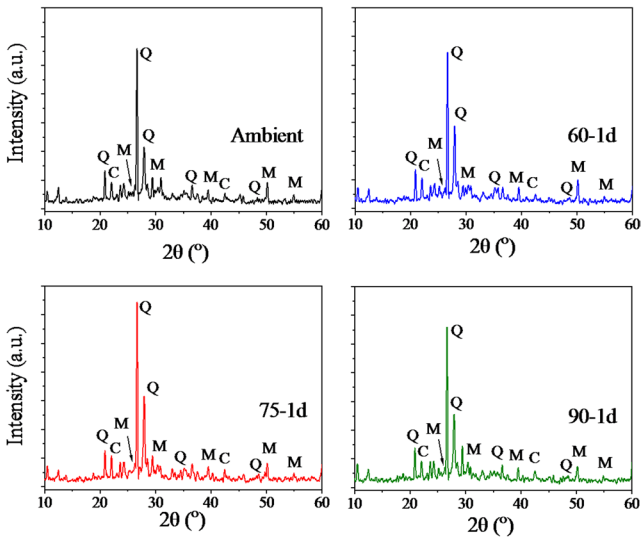


**Fig. 11** XRD patterns of Catalagzi FGPs at ambient, 60 °C, 75 °C, and 90 °C; M=mullite, Q=quartz, C=calcite

the raw fly ash appears as a broad hump within the 2θ range of 15° to 35° (Fig. 10), which is modified in the FGP pattern. This may be attributed to the consumption of reactive constituents from the amorphous fly ash during geopolymerisation, in agreement with the observations reported by Bai et al. [65]. In addition, several mullite-related reflections in the FGP pattern show lower apparent intensities than those in the raw fly ash, while the hematite-related reflections around 33° and 35° are no longer clearly distinguishable. Given the resistance of mullite to alkali dissolution under the curing conditions considered here [38], these differences are interpreted as qualitative variations in apparent peak intensity within the diffraction pattern. Quartz-related reflections remain visible in the FGP pattern, which may also be influenced by the sand used in mortar production. Taken together, these results suggest that geopolymerisation alters the diffraction pattern of the raw fly ash mainly through the consumption of reactive amorphous constituents.

XRD analysis was conducted to examine changes in the diffraction patterns with increasing curing temperature. Figure 11 shows the XRD patterns of Catalagzi FGPs cured for 1 day at ambient temperature, 60 °C, 75 °C and 90 °C. In comparison with Fig. 10, where the difference between the raw fly ash and the ambient-cured FGP is more evident, changes in the amorphous contribution are less clear when only the 1-day-cured FGP specimens are compared. This may indicate that, after 1 day of curing, the diffraction patterns remain broadly similar and that differences in reaction progress are still limited. Only minor changes are observed in the apparent intensities of some mullite-related reflections, while the more crystalline phases appear to remain comparatively stable under alkali conditions [38]. Quartz-related reflections remain visible despite the increase in temperature. This is consistent with Latifi et al. [78] and Turan et al. [4], who indicated that quartz behaves as an inert phase under alkaline conditions.

Figure 12 shows the XRD patterns of Catalagzi FGPs cured at 75 °C for 1 day and 7 days. With increasing curing time, only modest changes are observed in the relative intensities of several reflections. In addition, no clearly new crystalline phases are observed under the temperature conditions considered in this study. This is consistent with Duxson et al. [79], who reported that new crystalline phases are generally not expected at curing temperatures of 70–90 °C, whereas crystallisation may occur at higher temperatures, such as 120 °C.

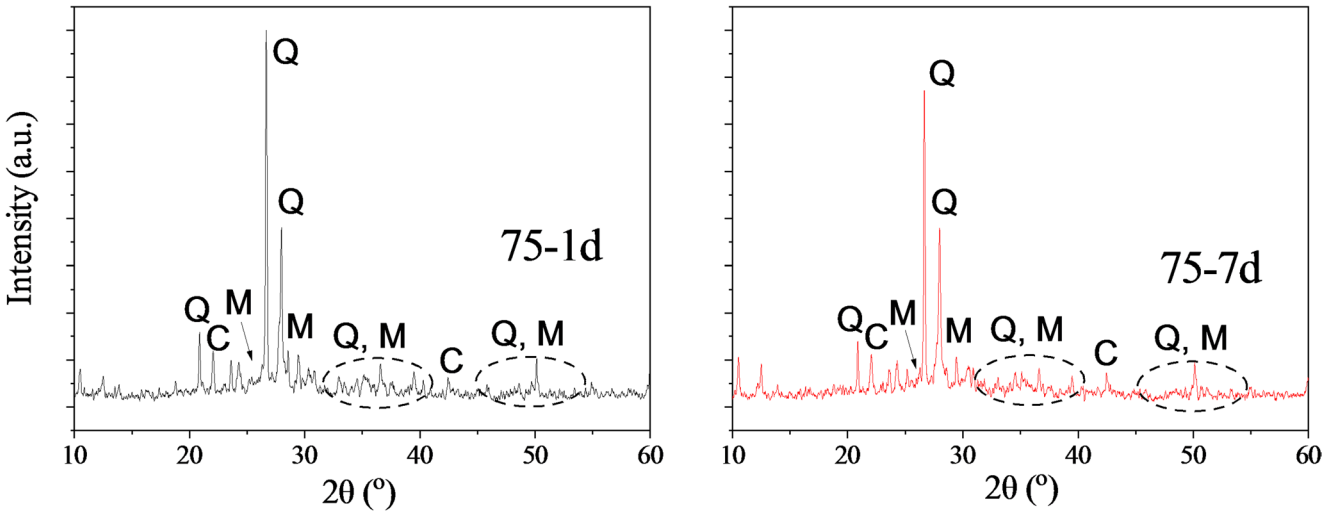


**Fig. 12** XRD patterns of Catalagzi FGPs cured at 75 °C for 1 and 7 days; M=mullite, Q=quartz, C=calcite

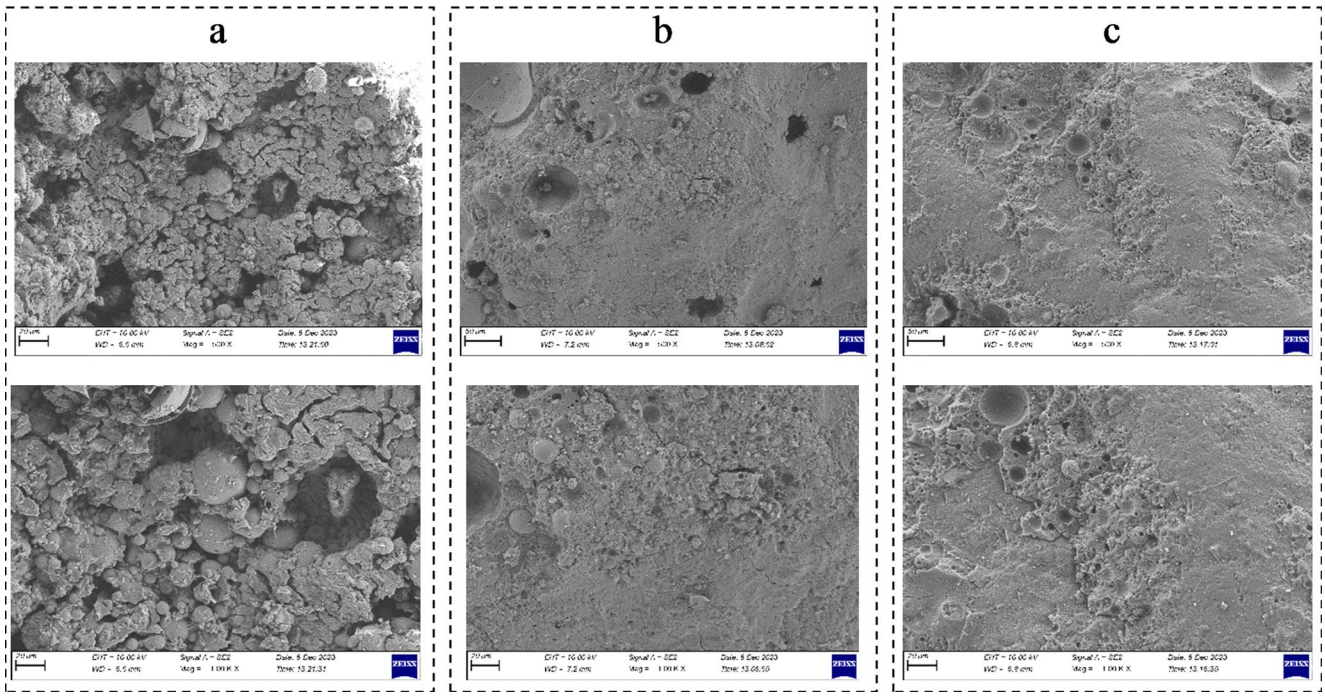


**Fig. 13** SEM micrographs of Catalagzi FGPs at different curing conditions: (**a**) AMB, (**b**) 75-1d, and (**c**) 75-7d

## Microstructural and Porosity Analysis

### Scanning electron microscope (SEM)

The SEM micrographs of Catalagzi FGPs are shown in Fig. 13. Samples cured at ambient temperature contain many unreacted fly ash particles. These particles decrease at a curing temperature of 75 °C. This indicates that highly amorphous fly ash dissolves in a high-alkaline environment, and its consumption rises with temperature. On the other hand, enhanced curing increases the number of fly ash particles with slightly reacted outer surfaces. In addition, Extending the curing duration to 7 days also increases these particles and the reaction rates on their surfaces. Thus, as curing temperature and duration increase, the outer glassy layers of the particles (thought to be cenospheres) join geopolymerisation reactions, while the crystalline outer layer stays intact [38, 46]. The low specific gravity of Catalagzi fly ash (2.13) indicates that many cenosphere particles, usually below 0.80 in specific gravity, exist in this raw material [46, 51, 80]. Although more fly ash particles react at higher curing temperatures and longer durations, some spherical particles

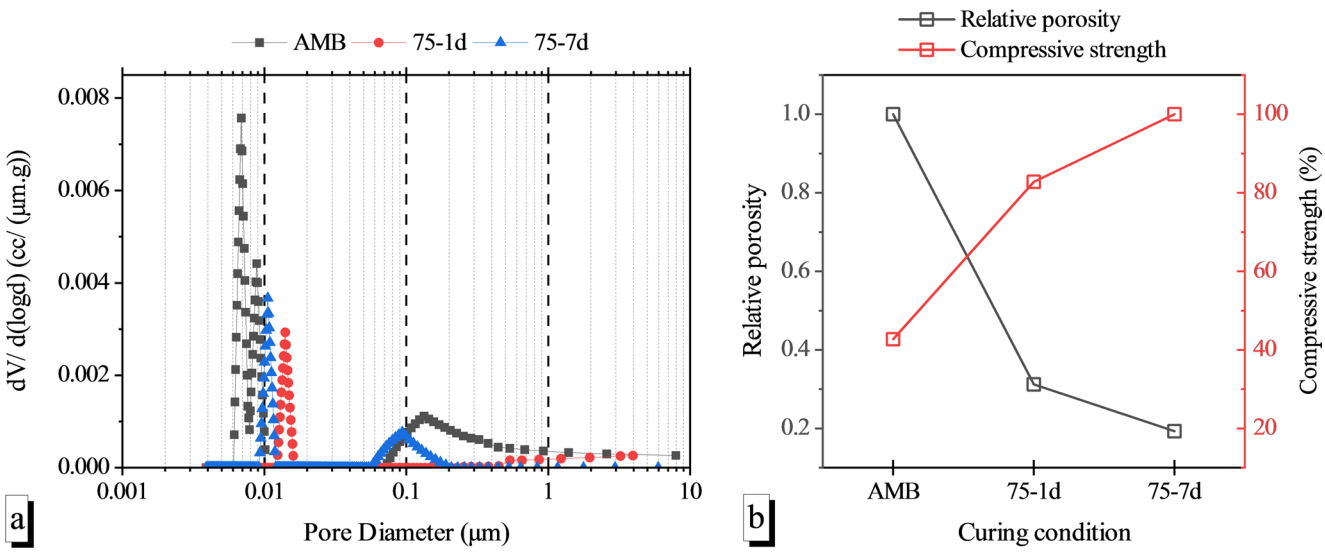


**Fig. 14** MIP results of Catalagzi FGPs: (**a**) differential pore size distribution; (**b**) correlation between total porosity and compressive strength

remain unreacted. These inert metal-oxide particles, which do not participate in geopolymerisation, may act as micro-aggregates and help prevent microcracks [79, 81]. However, in some cases, these rigid particles may also cause cracks in the hardened paste [68].

It can be observed that higher curing temperature and time allow geopolymer gels to fill pores and voids, creating a denser matrix. Yilmaz et al. [23] reported similar results and stated that higher curing temperature and time accelerate reactions, affecting reaction products and microstructure. As a result, more homogeneous and compact matrices form. Oz et al. [82] also noted that a denser microstructure increases compressive strength. Thus, the compressive strength results of this study align with the SEM findings.

### Mercury intrusion porosimetry (MIP) method

The polycondensation reactions in geopolymers are significantly influenced by curing time and temperature, as these factors alter the long-range arrangement of tetrahedral units. This change has a direct impact on the pore structure [83]. To observe the effect of the curing process on pore structure, MIP results of Catalagzi FGPs, which were also subjected to SEM analysis, are presented in Fig. 14(a). Furthermore, to establish a relationship between strength and porosity, the total porosity values obtained from this analysis are plotted against compressive strength in Fig. 14(b).

Pores in concretes are generally classified into four categories: micropores smaller than 10 nm, transitional pores between 10 and 100 nm, mesopores in the range of 100–1000 nm, and macropores larger than 1000 nm. Micropores are usually harmless, while transitional pores are considered slightly harmful. However, pores between 100 nm and 10 µm are linked to voids, cracks, and defects caused by unreacted particles, and are therefore considered detrimental [83–85].

As shown in Fig. 14(a), Catalagzi FGP cured at ambient temperature has a greater void volume for pores larger than 100 nm compared to heat-cured samples. This indicates that heat-curing reduces the size of larger voids. Zhang et al. [86] similarly reported that higher curing temperatures decrease the pore sizes in FGPs. Additionally, the total porosity of ambient-cured Catalagzi FGP is significantly higher than that of the heat-cured samples (Fig. 14(b)). This suggests that heat-curing promotes geopolymerisation, which reduces the size and connectivity of large voids.

On the other hand, extending the heat-curing duration at 75 °C from 1 day to 1 week slightly decreases the total porosity. This indicates that geopolymerisation reactions continue in Catalagzi FGP with longer heat-curing durations. As discussed in Sect. 3.2, the relatively low-reactivity of Catalagzi fly ash requires higher curing temperatures and longer durations for activation. In contrast, the high-reactivity of Sugozu fly ash achieves high strength at lower curing temperatures and shorter durations by completing (or maturing) its geopolymerisation. Considering the direct influence of pore structure on strength, it is expected that more refined pore structures can be achieved at lower curing temperatures and durations for highly reactive fly ashes like Sugozu.

## Conclusions and future perspectives

In this study, Class F fly ash based geopolymer (FGP) mortars were produced using fly ashes obtained from three different thermal power plants. The mortars were cured at various temperatures and durations to evaluate their performances. The strength development of Catalagzi FGPs from 3 to 90 days revealed that samples subjected to short-term heat-curing showed slower strength gain, whereas those cured at 60 °C and 75 °C revealed a significant increase in compressive strength over time. In contrast, prolonged curing (3 and 7 days) at 90 °C did not result in substantial additional strength gain. FTIR and XRD analyses indicated that increasing the curing temperature and duration enhanced the dissolution of Si and Al from the fly ash and increased the degree of cross-linking within the geopolymeric gel. Moreover, SEM images and MIP results confirmed that this intensified geopolymerisation process contributed to the formation of a denser matrix with reduced porosity, ultimately resulting in improved compressive strength.

The reactivity of fly ash is a key factor influencing the heat-curing requirements of FGPs to ensure sufficient geopolymerisation. FGPs produced with Sugozu fly ash, which exhibits relatively higher reactivity than other two fly ashes, achieved high strength even at lower curing temperatures and shorter durations. In contrast, the other two FGPs required more demanding curing conditions to reach comparable strength levels. In addition, the surface area of fly ash, shaped by its particle size distribution and morphology, plays a decisive role in determining the alkaline activator demand of FGPs. Owing to the predominance of uniformly spherical particles within a narrow size range, Sugozu FGPs required less alkaline activator during production. The combined effect of reduced heat-curing and lower activator demand in Sugozu FGPs is expected to decrease both $CO_2$ emissions and production costs compared with the other fly ash sources.

Future studies should also incorporate quantitative phase analysis, such as Rietveld refinement, in order to provide a more rigorous evaluation of the crystalline phases and amorphous content of different fly ashes. This would strengthen the interpretation of XRD results and improve the assessment of fly ash reactivity. In addition, further research should explore the scalability and real-world applicability of FGP concretes through life cycle assessments (LCA) and cost-benefit analyses. Such studies are crucial for facilitating the transition of these materials from laboratory research to market-ready sustainable construction products.

## References


1. Kürklü G (2016) The effect of high temperature on the design of blast furnace slag and coarse fly ash-based geopolymer mortar. Compos part b: Eng 92:9–18
2. Gopalakrishna B, Dinakar P (2023) The study on various temperature condition of fly ash based geopolymer mortar. Mater Today: Proc 93:234–238
3. Hardjito D, Cheak CC, Ing CHL (2008) Strength and setting times of low calcium fly ash-based geopolymer mortar. Mod Appl Sci 2(4):3–11
4. Turan C et al (2022) Effects of fly ash inclusion and alkali activation on physical, mechanical, and chemical properties of clay. Materials 15(13):4628
5. Turan C et al (2022) Geotechnical characteristics of fine-grained soils stabilized with fly ash, a review. Sustainability 14(24):16710
6. Abdullah HH, Shahin MA, Sarker P (2019) Use of fly-ash geopolymer incorporating ground granulated slag for stabilisation of kaolin clay cured at ambient temperature. Geotech Geol Eng 37:721–740
7. Corrêa-Silva M et al (2019) Improvement of a clayey soil with alkali activated low-calcium fly ash for transport infrastructures applications. Road Mater Pavement Des 20(8):1912–1926
8. Wong BYF, Wong KS, Phang IRK (2019) A review on geopolymerisation in soil stabilization. in IOP conference series: materials science and engineering. IOP Publishing
9. John SK, Nadir Y, Girija K (2021) Effect of source materials, additives on the mechanical properties and durability of fly ash and fly ash-slag geopolymer mortar: A review. Constr Building Mater 280:122443
10. Görhan G, Kürklü G (2014) The influence of the NaOH solution on the properties of the fly ash-based geopolymer mortar cured at different temperatures. Compos part b: Eng 58:371–377
11. Atiş C et al (2015) Very high strength (120 MPa) class F fly ash geopolymer mortar activated at different NaOH amount, heat curing temperature and heat curing duration. Constr building Mater 96:673–678
12. Zhuang XY et al (2016) Fly ash-based geopolymer: clean production, properties and applications. J Clean Prod 125:253–267
13. Gado R et al (2020) Alkali activation of waste clay bricks: Influence of the silica modulus, SiO2/Na2O, H2O/Na2O molar ratio, and liquid/solid ratio. Materials 13(2):383
14. Turan C (2023) Behaviour of clay stabilised with fly ash and alkali activated fly ash. University of Exeter
15. Li C, Sun H, Li L (2010) A review: The comparison between alkali-activated slag (Si+Ca) and metakaolin (Si+Al) cements. Cement concrete research. 40(9):1341–1349
16. Karaaslan C (2025) Unary, binary and ternary use of slag, nano-CaCO3, and cement to enhance freeze-thaw durability in fly ash-based geopolymer concretes. J Building Eng 99:111631
17. Dahale P, Nagarnaik P, Gajbhiye A (2017) Engineering behavior of remolded expansive soil with lime and flyash. Mater Today: Proc 4(9):10581–10585
18. Turan C, Javadi AA, Vinai R (2022) Effects of class C and class F fly ash on mechanical and microstructural behavior of clay soil—a comparative study. Materials 15(5):1845
19. Turan C et al (2019) Mechanical properties of calcareous fly ash stabilized soil. in Eurocoalash *2019*
20. Nawaz I (2013) Disposal and utilization of fly ash to protect the environment. Int J innovative Res Sci Eng Technol 2(10):5259–5266
21. Görhan G, Aslaner R, Şinik O (2016) The effect of curing on the properties of metakaolin and fly ash-based geopolymer paste. Compos Part B: Eng 97:329–335

22. Karaaslan C (2023) Enhancing Early Strength Development of Alkali-Activated Slag through Preheating of Materials, vol 38. Çukurova Üniversitesi Mühendislik Fakültesi Dergisi, pp 1129–1138. 4
23. Yılmaz A, Degirmenci FN, Aygörmez Y (2023) Effect of initial curing conditions on the durability performance of low-calcium fly ash-based geopolymer mortars. Boletín de la Sociedad Española de Cerámica y Vidrio
24. Yener E, Karaaslan C (2020) Curing Time and Temperature Effect on the Resistance to Wet-Dry Cycles of Fly Ash Added Pumice Based Geopolymer. Cem Based Compos 1(2):19–25
25. Karaaslan C, Şek Ş, Turan C (2025) Utilising High-Ambient-Temperature Curing in the Development of Low-Calcium Geopolymers. Buildings 15(16):2974
26. Somna K et al (2011) NaOH-activated ground fly ash geopolymer cured at ambient temperature. Fuel 90(6):2118–2124
27. Palomo A, Grutzeck M, Blanco M (1999) Alkali-activated fly ashes: A cement for the future. Cem concrete Res 29(8):1323–1329
28. Swanepoel J, Strydom C (2002) Utilisation of fly ash in a geopolymeric material. Appl Geochem 17(8):1143–1148
29. Criado M, Palomo A, Fernández-Jiménez A (2005) Alkali activation of fly ashes. Part 1: Effect of curing conditions on the carbonation of the reaction products. Fuel 84(16):2048–2054
30. Hardjito D, Rangan BV (2005) *Development and properties of low-calcium fly ash-based geopolymer concrete.*
31. Sindhunata et al (2006) Effect of curing temperature and silicate concentration on fly-ash-based geopolymerization. Industrial Eng Chem Res 45(10):3559–3568
32. Vora PR, Dave UV (2013) Parametric studies on compressive strength of geopolymer concrete. Procedia Eng 51:210–219
33. Adam AA, Horianto X (2014) The effect of temperature and duration of curing on the strength of fly ash based geopolymer mortar. Procedia Eng 95:410–414
34. Nagalia G et al (2016) Compressive strength and microstructural properties of fly ash–based geopolymer concrete. J Mater Civ Eng 28(12):04016144
35. Aliabdo AA, Elmoaty MA, Salem HA (2016) Effect of cement addition, solution resting time and curing characteristics on fly ash based geopolymer concrete performance. Constr building Mater 123:581–593
36. Zhang M et al (2018) Reaction kinetics of red mud-fly ash based geopolymers: Effects of curing temperature on chemical bonding, porosity, and mechanical strength. Cem Concr Compos 93:175–185
37. Hassan A, Arif M, Shariq M (2019) Effect of curing condition on the mechanical properties of fly ash-based geopolymer concrete. SN Appl Sci 1:1–9
38. Kuenzel C, Ranjbar N (2019) Dissolution mechanism of fly ash to quantify the reactive aluminosilicates in geopolymerisation. Resour Conserv Recycling 150:104421
39. Sajan P et al (2021) Combined effect of curing temperature, curing period and alkaline concentration on the mechanical properties of fly ash-based geopolymer. Clean Mater 1:100002
40. Rabie M, Irshidat MR, Al-Nuaimi N (2022) Ambient and Heat-Cured Geopolymer Composites: Mix Design Optimization and Life Cycle Assessment. Sustainability 14(9):4942
41. ASTM-C144-18 (2018) *Standard Specification for Aggregate for Masonry Mortar*, in *ASTM International*. West Conshohocken, PA, American Society for Testing and Materials
42. TS-EN-196-1 (2016) Çimento deney metotları - Bölüm 1: Dayanım tayini (Methods of testing cement - Part 1: Determination of strength). Ankara-Turkey, TSE
43. Sanalkumar KUA, Lahoti M, Yang E-H (2019) Investigating the potential reactivity of fly ash for geopolymerization. Constr Building Mater 225:283–291
44. Chen-Tan NW et al (2009) Determining the reactivity of a fly ash for production of geopolymer. J Am Ceram Soc 92(4):881–887
45. Pedersen KH et al (2008) A review of the interference of carbon containing fly ash with air entrainment in concrete. Progress Energy Combust Sci 34(2):135–154
46. Ranjbar N, Kuenzel C (2017) Cenospheres: A review. Fuel 207:1–12
47. Akgül Ç, Yoncacı S (2021) Türkiye Kömür Yakıtlı Termik Santral Uçucu Külleri (Fly Ashes from Coal-fired Thermal Power Plants in Turkey). Türkiye Çimento Sanayicileri Birliği Derneği
48. Sokol E et al (2000) Hollow silicate microspheres from fly ashes of the Chelyabinsk brown coals (South Urals, Russia). Fuel Process Technol 67(1):35–52
49. Danish A, Mosaberpanah MA (2020) Formation mechanism and applications of cenospheres: A review. J Mater Sci 55(11):4539–4557
50. Kavinkumar V, Priya A, Praneeth R (2023) *Strength of light weight concrete containing fly ash cenosphere.* Materials Today: Proceedings
51. Kolay P, Singh D (2001) Physical, chemical, mineralogical, and thermal properties of cenospheres from an ash lagoon. Cem Concrete Res 31(4):539–542
52. Rajamma R et al (2009) Characterisation and use of biomass fly ash in cement-based materials. J Hazard Mater 172(2–3):1049–1060
53. Mo B-h et al (2014) Effect of curing temperature on geopolymerization of metakaolin-based geopolymers. Appl Clay Sci 99:144–148
54. Zhang Z et al (2014) Using fly ash to partially substitute metakaolin in geopolymer synthesis. Appl Clay Sci 88:194–201
55. Kumar S, Kumar R (2011) Mechanical activation of fly ash: Effect on reaction, structure and properties of resulting geopolymer. Ceram Int 37(2):533–541
56. Hardjito D et al (2004) On the development of fly ash-based geopolymer concrete. Mater J 101(6):467–472
57. Karaaslan C et al (2022) Synergic effect of fly ash and calcium aluminate cement on the properties of pumice-based geopolymer mortar. Constr Build Mater 345:128397
58. Rovnaník P (2010) Effect of curing temperature on the development of hard structure of metakaolin-based geopolymer. Constr building Mater 24(7):1176–1183
59. Kamwa RAT et al (2023) Effect of Curing Temperature on Properties of Compressed Lateritic Earth Bricks Stabilized with Natural Pozzolan-Based Geopolymer Binders Synthesized in Acidic and Alkaline Media. Arab J Sci Eng 48(12):16151–16165
60. Muñiz-Villarreal M et al (2011) The effect of temperature on the geopolymerization process of a metakaolin-based geopolymer. Mater Lett 65(6):995–998
61. Aredes F et al (2015) Effect of cure temperature on the formation of metakaolinite-based geopolymer. Ceram Int 41(6):7302–7311
62. Hajimohammadi A, Provis JL, Van Deventer JS (2010) Effect of alumina release rate on the mechanism of geopolymer gel formation. Chem Mater 22(18):5199–5208
63. Hou Y et al (2009) Effect of activator and curing mode on fly ash-based geopolymers. J Wuhan Univ Technology-Mater Sci Ed 24:711–715
64. Heah C et al (2011) Effect of curing profile on kaolin-based geopolymers. Physics Procedia 22:305–311
65. Bai B et al (2023) A high-strength red mud–fly ash geopolymer and the implications of curing temperature. Powder Technol 416:118242
66. Gao R et al (2024) Innovative assessment of reactivity in fly ash: The role of particle size distribution characteristics. Open Ceram 20:100680
67. Salas DA et al (2018) Life cycle assessment of geopolymer concrete. Constr Building Mater 190:170–177

68. McLellan BC et al (2011) Costs and carbon emissions for geopolymer pastes in comparison to ordinary portland cement. J Clean Prod 19(9–10):1080–1090
69. Turner LK, Collins FG (2013) Carbon dioxide equivalent (CO2-e) emissions: A comparison between geopolymer and OPC cement concrete. Constr building Mater 43:125–130
70. Matsimbe J et al (2022) Geopolymer: A systematic review of methodologies. Materials 15(19):6852
71. Passuello A et al (2017) Evaluation of the potential improvement in the environmental footprint of geopolymers using waste-derived activators. J Clean Prod 166:680–689
72. Martinez A, Miller SA (2025) Life cycle assessment and production cost of geopolymer concrete: A meta-analysis, vol 215. Resources, Conservation Recycling, p 108018
73. Cong P et al (2024) Comparison and assessment of carbon dioxide emissions between alkali-activated materials and OPC cement concrete. J Traffic Transp Eng
74. Feng D, Provis JL, van Deventer JS (2012) Thermal activation of albite for the synthesis of one-part mix geopolymers. J Am Ceram Soc 95(2):565–572
75. Karaaslan C et al (2022) Improving the durability of pumice-fly ash based geopolymer concrete with calcium aluminate cement. J Building Eng 59:105110
76. Criado M, Fernández-Jiménez A, Palomo A (2007) Alkali activation of fly ash: Effect of the SiO2/Na2O ratio: Part I: FTIR study. Microporous mesoporous Mater 106(1–3):180–191
77. Pouhet R, Cyr M (2016) Carbonation in the pore solution of metakaolin-based geopolymer. Cem Concrete Res 88:227–235
78. Latifi N et al (2016) Strengthening montmorillonitic and kaolinitic clays using a calcium-based non-traditional additive: A micro-level study. Appl Clay Sci 132:182–193
79. Duxson P et al (2007) Geopolymer technology: the current state of the art. J Mater Sci 42:2917–2933
80. Satpathy H, Patel S, Nayak A (2019) Development of sustainable lightweight concrete using fly ash cenosphere and sintered fly ash aggregate. Constr Building Mater 202:636–655
81. Xu H, Van Deventer JS (2002) Geopolymerisation of multiple minerals. Miner Eng 15(12):1131–1139
82. Öz HÖ et al (2021) Process development of fly ash-based geopolymer mortars in view of the mechanical characteristics. Materials 14(11):2935
83. Chen S et al (2022) Pore structure of geopolymer materials and its correlations to engineering properties: A review. Constr Building Mater 328:127064
84. Wu R et al (2024) Effect of curing conditions on the alkali-activated blends: Microstructure, performance and economic assessment. J Clean Prod 445:141344
85. Liu W et al (2023) Comparative study on the performance of ultra-fine fly ash prepared by different techniques in Portland cement and alkali-activated material. Constr Building Mater 397:132362
86. Zhang Z et al (2014) Fly ash-based geopolymers: The relationship between composition, pore structure and efflorescence. Cem concrete Res 64:30–41